Chapter 9

Writing of Long Period Fiber Gratings Using CO_2 Laser Radiation

João M.P. Coelho, Catarina Silva, Marta Nespereira,
Manuel Abreu and José Rebordão

Additional information is available at the end of the chapter

http://dx.doi.org/10.5772/59153

1. Introduction

The development of optical fiber gratings (OFGs) had made significant advances both in terms of research and development of optical communications and sensors. OFGs are intrinsic devices that allow modulate the properties of light propagation within the fiber. Grating structures are comparatively simple and in its most basic form, consist on a periodic modulation of the properties of an optical fiber (usually the refraction index of the core). Its application as a sensing element is advantageous because of the intrinsic characteristics of the fiber sensors, such as remote sensing, electromagnetic immunity, weight and compactness, and capability for real time sensing and low cost [1].

Among OFGs, long period fiber gratings (LPFGs) are one of the most important fiber-based sensors. They were first presented by Vengsarkar and co-workers in 1996 [1] as band-rejection filters. Since then, LPFG technology has been receiving continuously growing attention from scientific community. Due to their spectral characteristics, LPFGs have found many applications in both optical communications and sensing systems. In the optical communications field, they have been demonstrated as gain equalizers [1], dispersion compensators [2], optical switches [3], components in wavelength division multiplexing (WDM) systems [4], band rejection filters and mode converters [5]. For optical sensing applications, LPFGs have been implemented as a temperature [6], strain [7] and refractive index sensor [8-10]. As element sensor a LPFG exhibits high sensitivity to the refractive index (RI) of the material surrounding the cladding surface. Other strengths are their low insertion losses, low back-reflection, polarization independence, relatively simple fabrication, and remote sensing easily multiplexed.

These gratings devices operate in transmission mode and are manufactured with periods typically in the range from 100 μm to 1000 μm [6]. Their large modulation period promotes the coupling of the light from the fundamental core mode to co-propagating cladding modes in a single-mode fiber [1]. The light coupled to the cladding decays quickly due to the absorption and scattering by the coating over the cladding.

A commonly-used optical fiber typically consists of a core and a cladding. In Figure 1 it is schematized the coupling mode that occurs in a LPFGs inscribed in single-mode fiber (SMF). As a result, the transmission spectrum of a LPFG has a series of resonant loss peaks (attenuation bands) centered at discrete wavelengths. A typical (theoretical) example is shown in Figure 2.

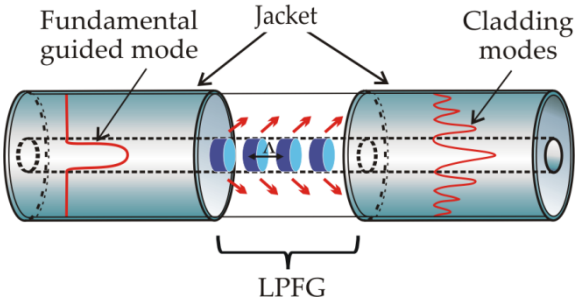

Figure 1. Schematic diagram of a mode coupling in a long period grating [11].

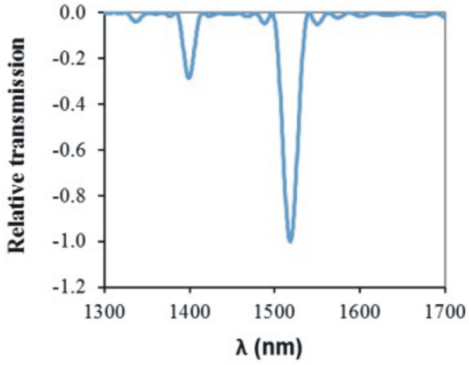

Figure 2. Theoretical example of the spectrum of a 500 μm-LPFG inscribed in a Corning SMF-28 fiber.

The resonant wavelength at which coupling takes place satisfies the phase matching condition

$$\lambda_{res}^{m} = \left(n_{eff,co} - n_{eff,cl}^{m}\right)\Lambda \tag{1}$$

http://dx.doi.org/10.5772/59153

in which $n_{eff,co}$ and $n_{eff,cl}$ are the effective refractive indices of the fundamental core mode and the m_{th} cladding mode, respectively; λ_{res} is the center wavelength of the transmission resonance; and Λ is the period of refractive index modulation [12].

Both resonant wavelength and attenuation amplitude of LPFGs are sensitive to a several physical parameters: temperature, strain, external refractive index, fiber dimensions, grating pitch, etc. These physical parameters affect the coupling between the core and cladding modes, which could lead to both amplitude and wavelength shift of the attenuation bands in the transmission spectrum [13]. The measurement of these spectral parameters in response to the environment surrounding the grating region is the basis of sensing with these devices.

In particular, LPFGs exhibits high sensitivity to changes in the RI of the medium surrounding the fiber due to the dependence of the phase matching condition upon the effective refractive index of the cladding modes. This characteristic makes these structures very attractive for sensing applications and several configurations, as well as applications, of LPFG devices for the measurement of physical and chemical quantities have been studied [6-13].

As mentioned before, LPFGs are created by inducing a periodic refractive index modulation (typically 10^{-4} [14-19]) in the core of an optical fiber with period lengths of several hundred micrometers. This can be made by permanent modification of the refractive index of the optical fiber's core or by physical deformation of the fiber.

Since the first demonstration of these devices by writing the grating with ultraviolet (UV) laser light through an amplitude mask in 1996 [1], several methods have been developed to create and improve the quality of the LPFGs. The conventional UV writing method is based on the exposure of photosensitive optical fibers to UV light through an amplitude mask, phase mask or by interferometry [8-9]. In germanium-doped (Ge-doped) silica fibers, UV light changes the refractive index of the core fiber, being this effect related with the formation of Ge-associated defects [20]. However, this method has some inherent limitations. It requires complex and time-consuming processes, including annealing and hydrogen loading for making the fibers photosensitive, and different amplitude masks when different dimensions are required. Also, the masks need replacement after prolonged usage and the required laser equipment is expensive.

There are, however, many non-photochemical methods available for gratings inscription. These include ion beam implantation [21], applying mechanical pressure [22], electric-arc discharge [23, 24] and irradiation by femtosecond laser pulses [25] or CO_2 laser beam [26, 27]. Among these methods, the latter is particularly flexible, as it can be applied to different types of fibers and the writing process can be computer-controlled to fabricate complicated gratings profiles without using amplitude masks. Furthermore, the use of infrared radiation as showed that the resulting interaction mechanisms are more efficient and allow creating devices with particular characteristics.

Taking this in consideration, this chapter addresses the application of CO_2 laser radiation in writing LPFGs and the physical principles involved in the process. A special emphasis will be given to the modulation of the refractive index resultant from the interaction between the mid-infrared (MIR) radiation (emitted by these lasers) and a conventional Ge-doped SMF.

In section 2 it will be described the fabrication process for applying the MIR radiation, starting with a review on the use CO_2 lasers in the creation of LPFGs. Experimental work is presented as well as the physical principles that may be responsible to induce the periodic refractive index modulation in the fiber's core.

Section 3 will address the subject of simulating the thermal mechanical processes involved in the process. Analytical and numerical models will be analysed and compared. In particular, a 3D finite element method (FEM) model will be presented, including the temperature dependence of the fiber's main parameters.

In section 4, it is presented a practical example of writing LPFGs on a Ge-doped fiber using a CO_2 laser. A comparison between calculated data and experimental data is made, and future work towards a full understanding of the physical processes is foreseen.

2. CO_2 laser induced LPFG

The use of CO_2 lasers to write LPFGs has emerged as an important alternative. Compared with other LPFG fabrication methods, this irradiation technique provides many advantages, including high thermal stability, more flexibility, lower insertion loss, lower cost. This section addresses the application of the CO_2 laser irradiation in creation of LPFG and the physical principles involved in this process.

The first results of the application of the 10.6 μm wavelength radiation emitted by CO_2 lasers for the fabrication of LPFG in a conventional fiber were published in 1998 [26-28]. Since then, different experimental methodologies have been described. The most common is the point-to-point technique using a static asymmetrical irradiation with a CO_2 laser emitting in a specific mode (continuous wave, CW, or pulsed) and a lens focusing the beam on the fiber. Akiyama [28] used continuous wave emission, while Davis [26] applied laser pulses with powers of about 0.5W.

In Figure 3 it is presented a schematic representation of a typical LPFG fabrication system based on the point-to-point technique employing a CO_2 laser. The optical fiber with its buffer stripped is placed on a motorized translation stage. In order to keep the fiber straight during the writing process, a small weight is applied at the end of the fiber and the laser beam is focused on the fiber. In this technique the periodicity of the LPFG writing is accomplished by moving the fiber along its axial direction via a computer controlled translation stage, which also controls the CO_2 laser beam emission. A broadband source and an optical spectrum analyzer (OSA) are employed to monitor the evolution of the spectrum during the laser irradiation. This method has the advantage of requiring a simpler setup, although the irradiation occurs on just one of the sides of the fiber. Also, the translation stage movement can generate vibrations that may be transmitted to the fiber, affecting the quality and repeatability of the LPFG. This problem can be solved using a system where the beam delivery system is moving instead of the fiber [29] or if the fiber is maintained static and a two-dimensional galvanometric mirrors system scans the beam over its surface [29-30]. Some authors reported

http://dx.doi.org/10.5772/59153

hybrid methods, combining point-by-point and scanning [31,32]. In this chapter we will consider the method presented by Alves *et al.* [32] that combines a translation stage to move the fiber synchronized with a one-dimensional scan over a cylindrical lens.

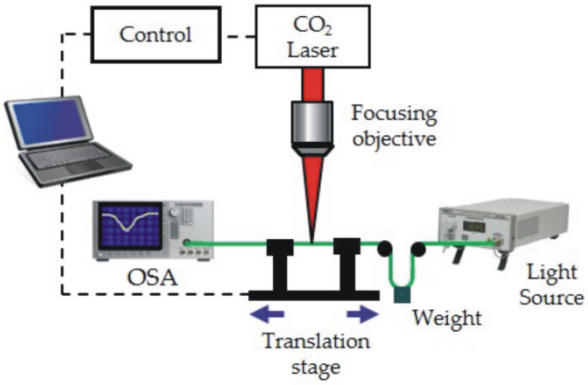

Figure 3. Schematic diagram of a typical LPFG fabrication system based on the point-to-point technique using a CO_2 laser.

Since the silica glass has strong absorption around the wavelength of the CO_2 laser radiation, the beam intensity is gradually attenuated along the incident direction, resulting in asymmetric RI modulation. Such distribution could cause coupling of the core mode to both the symmetric cladding modes and the asymmetric cladding modes [33]. As a result, high fiber grating birefringence and high polarization-dependent loss can become inevitable [30].

In order to solve the birefringence problem, different methods have been proposed. Single–side and symmetric exposures to the laser radiation were compared by Oh *et al.* [34], demonstrating that the polarization-dependent loss of the single-side exposure (1.85 dB at 1534 nm) could be significantly reduced to 0.21 dB by applying the second method. Nevertheless, due to its simplicity, the single-size exposure is the most common applied methodology. Grubsky [35] proposed a simple fabrication method for obtaining high-quality LPFGs with a CO_2 laser using a reflector to make the fiber's exposure axially uniform. Zhu *et al.* [36] used a high frequency CO_2 laser system to write LPFGs with uniform RI modulation by introducing twist strains to the fiber and then exposing the two sides of the fiber to the laser radiation. Experimental results showed that twisted LPFGs (T-LPFGs) exhibited clear spectra, low insertion losses, and low polarization-dependent losses when compared with those created by exposure to a single-side CO_2 laser beam [37].

Gratings inscription was also achieved through the use physical deformations (or geometrical deformation). Wang *et al.* [38] proposed a new method for writing an asymmetric LPFG by means of carving periodic grooves on one side of a fiber with a focused CO_2 laser beam. The periodic grooves do not cause a large insertion loss because these grooves are totally confined within the cladding and have no influence on the light transmission in the fiber's core. The

grooves enhance the efficiency of grating fabrication and introduce unique optical properties (extremely high strain sensitivity). In 2006, Su *et al.* [39] demonstrated the possibility of producing long-period grating in multimode fibers by deforming the geometry of the fiber periodically with a focused CO_2 laser beam and applied them to strain measurements.

Besides conventional single-mode fibers (SMFs), CO_2 laser have been used to write LPFGs in other types of fiber, such as boron doped SMF [40,41], and photonic crystal fibers (PCFs) [42,44].

There have been many studies focused on the understanding of the physical mechanisms involved in the CO_2 laser writing process for different kinds of fibers. Most of the existing works consider that the main mechanisms responsible for creating a refractive-index change in the CO_2 laser irradiation-induced LPFGs are residual stress relaxation processes [26,29,35,40-44]. In these processes, heat created by the absorption of laser energy in the material play an important role and, as will be explained next, modelling the writing process requires considering both thermal and mechanical processes.

3. Thermo-mechanical modelling

As mentioned before, the main effect behind LPFG fabrication using CO_2 lasers is heating, where the refraction index change is achieved by irradiating a fiber submitted to a tensile stress. The high absorption of the glass material to the MIR radiation emitted by these lasers leads to an excess of energy due to the excitation of the lattice which is transformed into heat, increasing the material's temperature from its surface to its bulk by heat conduction. This effect depends on the irradiation time and on the thermal diffusivity of the material, it is localized and periodically induced in the fiber's length, being responsible for the creation of the gratings.

Considering the temperature, T, changing with time, t, (transient regime) due to the action of a heat source $Q(r,t)$, the resulting energy balance leads to the heat conduction equation:

$$\left[\frac{\partial \rho}{\partial t} + \rho \nabla \cdot \vec{u}\right] \int C_p \, dT + \rho C_p \left(\frac{\partial T}{\partial t} + \vec{u} \cdot \nabla T\right) - \nabla \cdot K \nabla T = q(T) + Q(r,t) \tag{2}$$

where r represents the geometric coordinates (depending on the geometry) and being ρ the density, $\bar{u}$ the velocity vector, C_p the specific heat and K the thermal conductivity. The convective and radiative heat flux is represented by [45]:

$$q(T) = h\left(T_{ext} - T\right) + \sigma_B \, \varepsilon \left({T_{amb}}^4 - T^4\right) \tag{3}$$

being T_{ext} the external temperature, T_{amb} the ambient temperature, h the heat transfer coefficient, σ_B the Stefan-Boltzmann constant and ε the surface emissivity.

If enough energy is applied, differences in the thermal expansion coefficients and viscosity of core and cladding lead to residual thermal stresses and draw-induced residual stresses, and

http://dx.doi.org/10.5772/59153

refractive index change results from frozen-in viscoelasticity [46]. The analysis of these effects is complex and highly dependent on the physical characteristics of the different materials composing the optical fiber. For simplifying the subject, we will consider silica-based single mode fibers since they are at the base of most LPFGs manufactured using CO_2 lasers. Also, from the different irradiation methodologies explained in the previous section, we will consider the coordinate referential illustrated in Figure 4. The main interfaces between regions of interest in the fiber, illustrated in Figure 4(b), are represented by a point in the upper surface (relative to laser incidence), two points in the cladding/core interface and one point in the bottom interface. In order to simplify the plots regarding calculated data in section 4, and since early work demonstrated low variation in temperature between the cladding/core interfaces [47-49], we use the core's middle point instead.

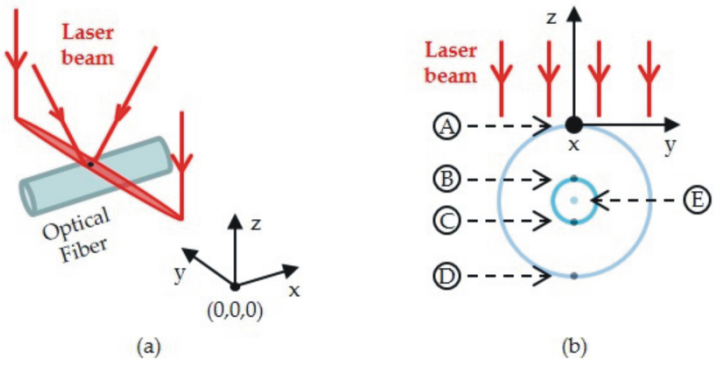

Figure 4. (a) Schematic of coordinates used in this work and (b) optical fiber cross-section indicating the considered referential, the interfaces between the different regions, and points of interest: A – irradiated surface, B – core/cladding interface (upper), C – core/cladding interface (lower), D – bottom surface and E – middle point. The origin of the reference system is in the middle of the laser line.

3.1. Laser heating modelling

When considering an homogeneous isotropic material, the condition of mass conservation, and introducing the thermal diffusivity k, given by $K/(\rho C_p)$, Equation (2) can be simplified to:

$$\left(\frac{\partial T}{\partial t}+\vec{u}\cdot\nabla T\right)-k\nabla\cdot\nabla T-q(T)=\frac{Q(r,t)}{\rho C_p} \tag{4}$$

For a laser beam incident on a surface and propagating in the z-direction:

$$Q(r,t)=a_T(1-R)I(r)\varphi(t) \tag{5}$$

where a_T is the attenuation coefficient of the material, R its reflectance and $I(r)$ the irradiance. For continuous wave emission with a duration t_{on}:

$$\varphi(t)=\begin{cases}0, \text{if } t\le 0 \vee t>t_{on}\\ 1, \quad \text{if } 0<t\le t_{on}\end{cases} \tag{6}$$

Accordingly with the irradiation geometry schematized in Figure 4, and considering that the laser beam has an elliptical Gaussian distribution at the surface being irradiated, then [50]:

$$I(r)=I(x,y,z)=\frac{2a_T P}{\pi r_x r_y}\exp\left[-2\left(\frac{x^2}{r_x^2}+\frac{y^2}{r_y^2}\right)-a_T|z|\right] \tag{7}$$

where r_x and r_y are the values of the ellipse's semi-minor and semi-major axis, respectively.

If one neglects radiative and convective losses and considers temperature dependent material properties, then it is possible to obtain analytical expressions to the temperature. Typically [47,50,51], the heat equation is solved numerically using the Green's function method and the temperature can be obtained [49]:

$$\begin{aligned}T(x,y,z,t)=\frac{(1-R)P}{4\pi K r_x r_y}\int_0^{\sqrt{4kt}}\Psi(x,y,s)\cdot\Bigg[&\exp(a_T|z|)\,erfc\left(\frac{a_T s}{2}+\frac{|z|}{s}\right)+\\&+\exp(-a_T|z|)\cdot\sqrt{a^2+b^2}\cdot erfc\left(\frac{a_T s}{2}-\frac{|z|}{s}\right)\Bigg]ds\end{aligned} \tag{8}$$

with

$$\Psi(x,y,s)=\frac{a_T s}{\dfrac{s^2}{(r_x r_y)}+1}\cdot\exp\left[\frac{x^2}{r_x^2+s^2}-\frac{y^2}{r_y^2+s^2}+\frac{(a_T s)^2}{4}\right] \tag{9}$$

From (8) an on-axis approximation can be used [51] and the temperature rise can be approximated through simple analytical expressions:

$$\Delta T(0,0,\infty)=\frac{(1-R)P}{2\sqrt{\pi r_x r_y}K} \tag{10}$$

http://dx.doi.org/10.5772/59153

for the steady state condition ($t >> r_x^2\, r_y^2 / 4k$) and

$$\Delta T(0,0,t) = \frac{(1-R)P}{\pi^{3/2} K \sqrt{r_x\, r_y}} \tan^{-1}\left(\sqrt{\frac{4kt}{r_x\, r_y}}\right) \tag{11}$$

under transient conditions. Although Yang *et al.* [51] proved that these equations can be used to study the thermal transport in CO_2 laser irradiated fused silica, when modelling the effects in writing LPFGs, the full 3D temperature distribution is required and a numerical approach is mandatory [48]. Using a dedicated Finite Element Method (FEM) program, although computationally demanding, allows not only considering all the physical phenomena, but also including the temperature dependence of the materials and even the simulation of consecutive periods. If two laser shots are considered, one centred in (0,0,0) and at t=0 s, and the other at $x=\Delta x$ and $t=t_2=t_{on}+\Delta t$. In the latter case ($t=t_2$), equations (6) and (7) are altered accordingly to

$$\varphi(t') = \begin{cases} 0, \text{ if } t' \le 0 \vee t' > t_{on} \\ 1, \quad \text{if } 0 < t' \le t_{on} \end{cases}, \text{ with } t' = t - (t_{on} + \Delta t) \tag{12}$$

$$I(r) = I(x,y,z) = \frac{2a_T P}{\pi r_x\, r_y} \exp\left[-2\left(\frac{(x-\Delta x)^2}{r_x^{\,2}} + \frac{y^2}{r_y^{\,2}}\right) - a_T |z|\right] \tag{13}$$

3.2. Residual elastic stresses modelling

Residual elastic stresses are considered those that are frozen into the fiber [52] and have an important impact on the production of LPFG since they affect the refractive index of an optical fiber. When using the considered MIR radiation, two categories of residual elastic stresses must be considered: thermal and draw-induced stresses.

3.2.1. Residual thermal stresses

Residual thermal stresses appear as the optical fiber is cooled down from high temperatures and regions with different thermal expansion coefficients contract differently in time. Dopants introduced increase the differences in viscosity and thermal expansion coefficients.

A solution for the resulting residual thermal stresses of an initially unstressed axisymmetric cylinder heated at a given temperature, T, can be obtained using the radial coordinate r [52,53]

$$\sigma_x = \frac{E}{1-\nu}\left[\frac{2\nu}{r_c^2}\int_{r=0}^{r_c} \alpha T r dr - \alpha T\right] \tag{14}$$

$$\sigma_r = \frac{E}{1-\nu}\left[\frac{1}{r_c^2}\int_{r=0}^{r_c} \alpha T r dr - \frac{1}{r^2}\int_{r=0}^{r} \alpha T r dr\right] \tag{15}$$

$$\sigma_\theta = \frac{E}{1-\nu}\left[\frac{1}{r_c^2}\int_{r=0}^{r_c} \alpha T r dr + \frac{1}{r^2}\int_{r=0}^{r} \alpha T r dr - \alpha T\right] \tag{16}$$

being r_c the radius (cladding or core), E the Young's modulus and υ the Poisson's ratio. This solution is valid when the elastic properties can be considered constant, which doesn't applies for optical fibers. Thus, and similarly to the approximated solution for heating, given by equations (8) and (9), not taking in consideration the temperature dependence of the different parameters can lead to non-accurate results. Again, the use of numerical methods, with particular focus on FEM, are appropriated and give the opportunity to combine both heating and thermal stresses models. In this case, by solving equation (4), the thermally-induced residual stresses, σ_T, can be obtained considering the constitutive equations for a linear isotropic thermoelastic material and the stress tensor obtained.

3.2.2. Draw-induced stresses

Residual stress effects on the refractive indices of fibers were reported for the first time by Hibido *et al.* in 1987 [54,55] regarding undoped silica-core single mode fibers. Considering a fiber with core and cladding, having different viscosities due to different dopants concentrations, during the draw process the higher viscosity glass will solidify first and support the draw tension. The low-viscosity glass solidifies conforming with the elastically stretched high-viscosity glass. Then, when the draw force is released at room temperature, the high-viscosity glass cannot contract due to the already solidified low-viscosity glass. The resulting residual axial elastic stresses can be expresses as

$$\sigma_{x,1} = F\left(\frac{E_1}{A_1E_1 + A_2E_2}\right) \tag{17}$$

and

$$\sigma_{x,2} = \frac{F}{A_2}\left(\frac{A_1E_1}{A_1E_1 + A_2E_2}\right) \tag{18}$$

being F the draw tension, A the cross-section area and E the Young's module for the considered regions. The indexes 1 and 2 in these equations represent the regions of low-viscosity and high-viscosity glasses, respectively.

http://dx.doi.org/10.5772/59153

Similarly to these stresses, frozen-in inelastic strains were also found if a fiber is rapidly cooled to room temperature while under tension (as in the considered case) [46,52]. Using the equivalent elastooptic relations [52], the isotropic perturbation on the refractive, Δn, index is

$$\Delta n = -\frac{n^3}{6}\chi\left(T_F\right)p\sigma \tag{19}$$

In the later expression, n is the nominal refractive index, $\chi(T_F)$ is the relaxation compressibility at the fictive temperature, T_F, p is the orientation average elastooptic coefficient, and σ the overall residual stresses (in MPa) in the fiber's axial direction. Accordingly with Yablon [52], stresses in the other directions can be neglected.

Besides stress-related refractive index change, localized heating can induce micro-deformation of the fiber and changes in the glass structure. The latter is likely to occur in the core for which the fictive temperature (the glass structure doesn't change below the fictive temperature) is lower [56,57]. As reported for a Ge-doped core (e.g. the fictive temperature ranges from 1150 K to 1500 K.

4. A practical example

To illustrate the application of the theory and also correlate it with experimental data, we will consider a common example of LPFG writing using NIR radiation: a standard single-mode fiber, SMF-28 [58], consisting of a core of 3.5 mol% Ge-doped SiO_2, is irradiated by a CW 10.6 μm wavelength CO_2 laser. For fused silica, $n \approx 1.45$ (in the near-infrared), $\chi(T_F) \approx 0.0568$ GPa^{-1} and $p \approx 0.22$, which allows simplifying equation (19):

$$\Delta n \approx -6.35\times10^{-6}\,\sigma \tag{20}$$

Also, in this case, equations (17) and (18) represent, respectively, the residual axial elastic stresses at the core (low-viscosity glass) and the cladding (high-viscosity glass) [46].

The particular conditions used in both simulation and experimental works, as well as the obtained results, will be detailed next.

4.1. Simulation

The simulation of the writing process was made implementing a 3D FEM model using the COMSOL Multiphysics program. Whenever relevant, the material's dependence with temperature was considered and the proper geometry and FEM parameters defined.

Besides COMSOL, two other programs were used: Matcad and a simulation tool developed in MatLab by Baptista [60] based on the three layer model developed by Erdogran [14,60]. The

latter was used to apply the refractive index data obtained in the FEM model to simulate the transmission spectrum of a LPFG. Matcad was used to solve equations (8) and (11) and compare the temperature data with that obtained through the FEM model.

4.1.1. Fiber's characteristics

When light interacts with matter, one of the main parameters is the absorption coefficient, a_T. As it can be deduced from the formulae of section 3, it plays a major role in the process of heating the fiber. Besides its dependence with the wavelength of the light, it varies with temperature. This variation is important and for the 10.59 μm CO_2 laser wavelength (λ_1), within 298 K–2,073 K temperature range can be obtained by [61]:

$$a_T(T) = \frac{4\pi}{\lambda_1}\left[1.82\times10^{-2} - 10.1\times10^{-5}(T - 273.15)\right] \tag{21}$$

For the thermal conductivity, heat capacity, density and emissivity, the temperature dependence was modelled using native COMSOL functions for a Corning fused silica glass (7940) [48]. The doping effect on most of the parameters was disregarded mainly because the Ge concentration in the fiber's core is very low [62]. However, for the Young's modulus and Poisson's ratio (Figure 5), the function behaviour was extrapolated [63]. Also, both the heat transfer coefficient and reflectivity were considered constant and equals to 418.68 W m^{-2} K^{-1} [45] and 0.15 [51], respectively.

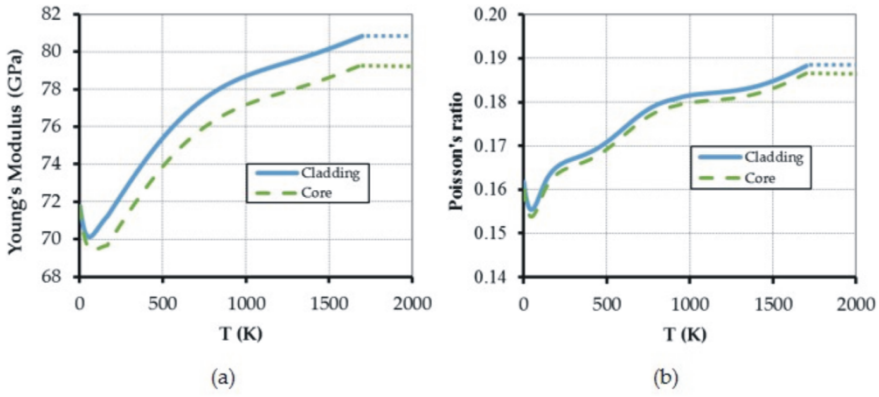

Figure 5. Variation of (a) Young's module and (b) Poisson's ratio with temperature for both fused silica (from COMSOL materials library) cladding and Ge-doped fused silica (extrapolated) core glasses.

http://dx.doi.org/10.5772/59153

4.1.2. Implementation

The physical problem was mathematically solved using the FEM model implemented using the COMSOL Multiphysics 3.5 program to create the transient heat conduction and (mechanical) stress-strain models under the conditions of this study. In order to introduce some of the complexity of stress-related issues regarding the processing of the optical fibers, the residual axial elastic stresses were implemented considering Equations (9) and (10) and the total resulting stress was obtained adding the thermally-induced residual stresses obtained with the program.

As illustrated in Figure 4, the implemented geometry consists of a set of (concentric) cylinders with radius of curvatures accordingly with the characteristics of the core and cladding of the fiber previously described. To avoid the influence of the external boundaries on the irradiated and analysed zones, the overall length for the geometry was set as 13 mm. However, to reduce the computational load and loosen the mesh dimensions in the volumes not affected heat source, the cylinders were implemented as three separate sets; the central one, where the laser incidence will be simulated, has a 1.7mm length. The outer set of cylinders are asymmetric since the second laser shot will be simulated just in the positive x-direction.

Table 1 presents the 3D geometry data and the mesh statistics and Figure 6 shows the implemented mesh, with particular focus on the central irradiation zone. Both outer boundary surfaces are defined as thermally isolated, being one of them fixed. The ambient temperature was considered to be 295 K and equal to the external temperature, T_{ext} in Equation (3).

	Central geometry		**External geometries**			
	Cladding	**Core**	**Cladding**		**Core**	
Geometry			Left	Right	Left	Right
Length (mm)	1.7		5.15	6.15	5.15	6.15
Radius (μm)	62.5	4.1	62.5		4.1	
Mesh (tetrahedral)						
# elements	26,122	1,795	26,262	26,825	1,710	1,795
min. quality	0.0495	0.1659	0.2287	0.2284	0.2004	0.1956
volume ratio	8.47×10^{-4}	0.1010	0.0028	0.0036	0.4906	0.3593

Table 1. Geometry data and mesh statistics.

Figure 6. Image of the mesh implemented at the central zone of the FEM geometry. The coloured region corresponds to the central geometry with finer mesh (Table 1).

4.2. Experimental methodologies

The implemented irradiation methodology combines a translation stage to move the fiber synchronized with a one-dimensional scan over a cylindrical lens [32]. Figure 7 shows a schematic of the setup and Figure 8 a picture of its implementation. The light source is a Synrad 48-2 CO_2 laser emitting a 3.5 mm diameter CW laser beam with a wavelength of 10.6 μm. Two mirrors direct the beam towards the focusing lens, a ULO Optics ZnSe cylindrical lens (50 mm focal length) which produces a 0.15 mm x 1.75 mm (measured using the knife-edge method [64]) elliptical spot on the fiber with its longer axis perpendicular to the fiber's axis. One of the mirrors is a galvanometric mirror (Cambridge Technology 6860) which allows a scan over the lens (and, consequently, over the surface of the fiber).

A linear translation stage moves axially the fiber so the periodic refractive index change is accomplished. During the process, one of its ends is fixed and a weight (typically ~50 g ± 0.5 g) hangs on the other, thus creating a tension. Thus, this system acts like a XY writing system. The advantage of the translation stage is its long range with micrometric precision (10 cm with a repeatability of 1 μm). However, it has the disadvantage of having relative low speed when compared with a galvanometric system. Combining the two systems, we have the benefit of having a long X-axis range with a fast Y-axis range and, by moving the laser spot very fast over the fiber (Y-axis), lower interaction times can be achieved. Also, since the laser is not always over the fiber, it's possible to have the laser emitting continuously, which prevents the transients during the laser start-up and allows easier control of its power. Uncertainties regarding the irradiation data are: power, ±0.5 W; duration, ±1 ms.

To monitor the LPFG fabrication process, a broad band light source (Thorlabs S5FC1005S) and an OSA (Agilent 86140B) were used. The irradiated zones were analysed using an optical microscope (Zeiss AxioScope A1) with a maximum amplification of 1,000×. The LPFG period is limited by the laser spot size and by the translation stage minimum movement. In the considered setup, since the translation stage can have 1 μm steps, the laser spot size (150 μm) constitutes the major limitation.

http://dx.doi.org/10.5772/59153

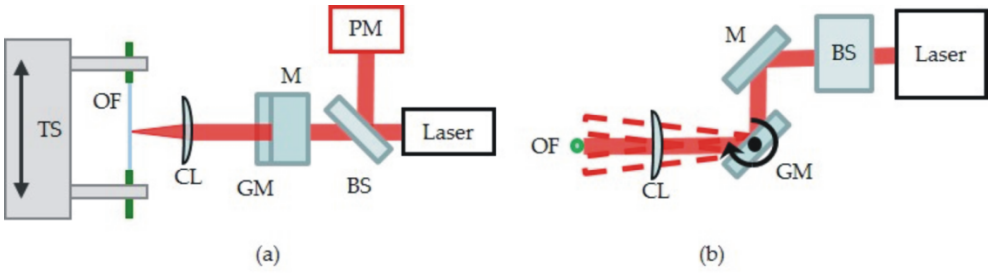

Figure 7. (a) Top and (b) lateral schematic views of the optical setup. BS – beam splitter; CL-cylindrical lens; GM – galvanometric mirror; M – mirror; OF – optical fiber; PM – power meter; TS – translation stage.

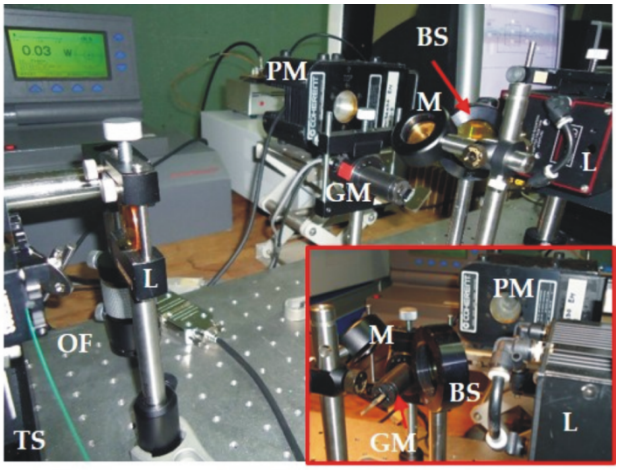

Figure 8. Picture of the setup implemented. The inset shows a detail view of the laser output area. BS – beam splitter; CL – cylindrical lens; GM – galvanometric mirror; L – laser; M – mirror; OF – optical fiber; PM – power meter; TS – translation stage.

4.3. Results and analysis

An example of the temperature distribution resulting from considering 6 W laser power, irradiation duration of 0.6 s and 47 g weight (F=0.461 N) is shown in Figure 9(a). The result of simulating a second irradiation (equivalent to have a LPFG period), 1 s after the first, at a distance of 500 μm, is shown in Figure 9(b).

Figure 10 shows the equivalent plots of temperature with time for the irradiated front, core (middle) and the back surfaces (Figure 4), at x=y=0 m and x=500 μm, y=0 m. These plots show that the (spatial) proximity between shots raises the temperature even when they are not under direct irradiation. As the distance reduces (shorter LPFG periods), this secondary heating increases (Figure 11). This is particularly important when the second shot is applied because

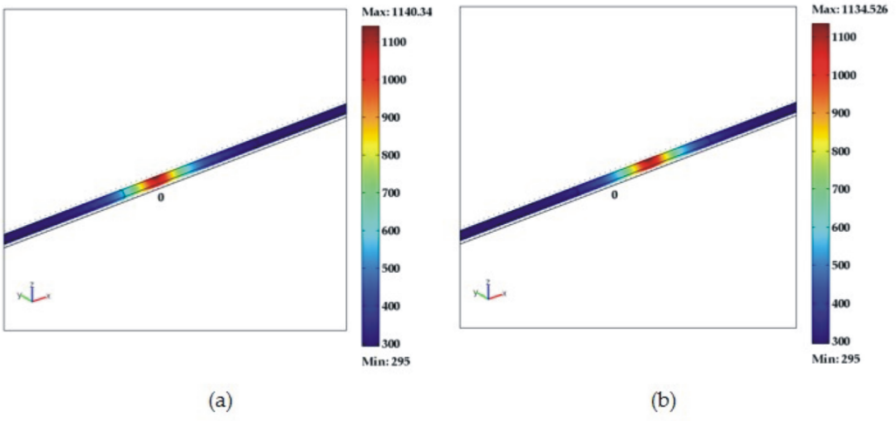

Figure 9. Temperature distribution in the implemented 3D geometry for the laser irradiation of an optical fiber (P=6 W; t_{on}=0.6 s; F=0.461 N; Δt=1 s; Δx=500 μm), at (a) t=0.6 s and (b) t=2.2 s. Colour bar values are in K.

of the possibility of annealing, which could (totally or partially) relieve the previously induced internal stresses.

Similarly, as we analyse the temperature distribution at the fiber's axial direction plotted in Figure 12(a) (for the same conditions of Figure 10), the superposition of thermally affected areas in both shots underlines one critical aspect when writing LPFGs: the influence of the grating's period on the pitch width, and consequent "softening" of the spatial refractive index gradient. As it can be seen in Figure 12(b), as the period decreases, the interception's x-coordinate values decreases and the temperature at that point increases.

The practical consequence of this behaviour it's not clear at this time and further research is necessary, but these phenomena can be responsible by the reduction of the success rate in producing LPFGs with shorter periods found in other studies [65].

The importance of using the FEM simulation instead of the analytical equation (11) or the approximated integral equation (8) is observed in Figure 13 for the temperature at the core (middle). In fact, disregarding radiative and convective losses, adding to the important variation on the parameters values with temperature, deviates the solution by a significant amount (about 200 K at its maximum values, between each solution).

As expected, as the laser power increases, the temperature also increases. From the data obtained using the FEM model and plotted in Figure 14, a 3rd order polynomial can be used to relate these two parameters. Considering

$$T(P) = a_3 P^3 + a_2 P^2 + a_1 P + a_0 \tag{22}$$

http://dx.doi.org/10.5772/59153

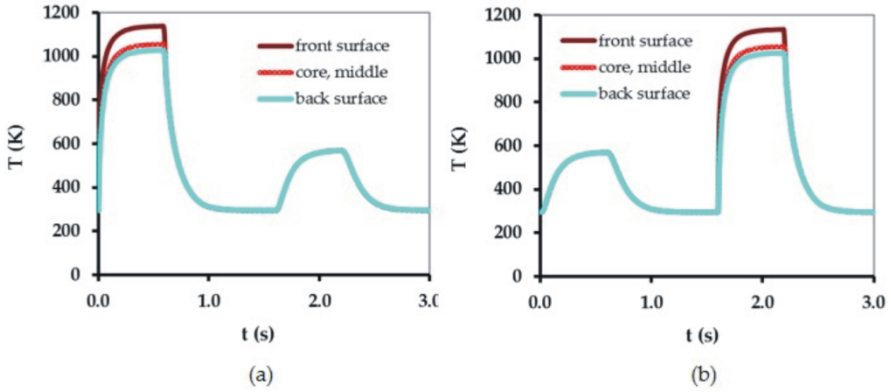

Figure 10. Plots of the temperature evolution during laser irradiation and cooling at (a) x=0 m and (b) x=Δx. (P=6 W; t_{on}=0.6 s; F=0.461 N; Δt=1 s; Δx=500 μm).

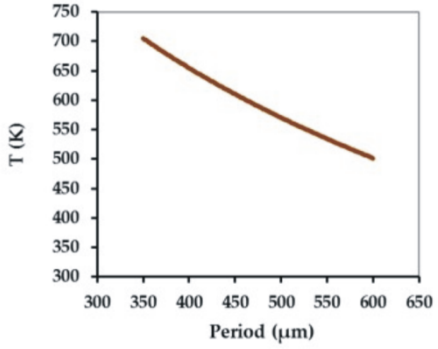

Figure 11. Maximum temperature at x=0 m when the laser is irradiating at x=Δx for different values of Δx (LPFG period). (P=6 W; t_{on}=0.6 s; Δt=1 s; F=0.461 N).

(with the laser power, P, in W, and the temperature, T, in K), Table 2 gives the equivalent parameters for the different zones of the fiber.

For the considered example, at t=0.6 s, axial residual thermal stresses values along z-axis were determined as having a maximum of about −0.8 MPa. Axial elastic stresses act in the opposite direction and were calculated as being $\sigma_{x,1}$=35 MPa and $\sigma_{x,2}$=0.153 MPa. This results in refractive index changes (difference between final and initial values) for the core and cladding of the order of -2×10^{-4} and 4×10^{-6}, respectively. Figure 15 shows the calculated (maximum) changes for different laser power. Under the considered conditions, it is clearly observed that for the cladding, a well-defined step occurs between 4.5 W and 5 W. Regarding the core, although its refractive index shows minor variations, it is possible to observe the beginning of the contribution of thermal stresses around 5 W.

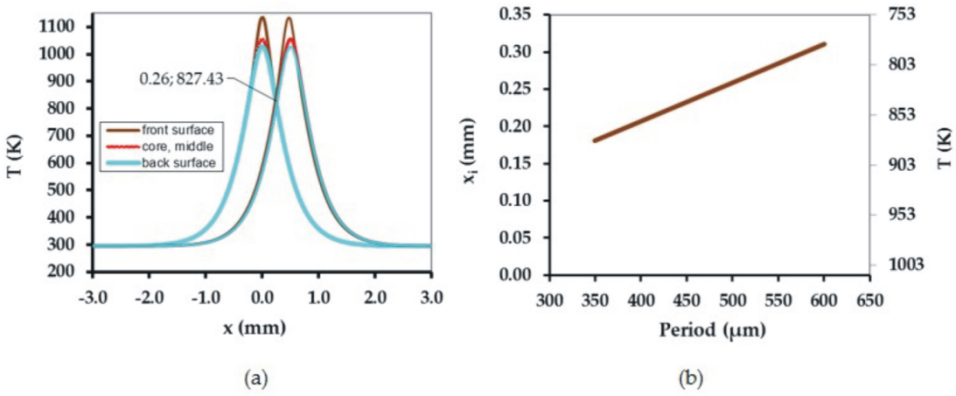

Figure 12. (a) Plots of the temperature distribution at the fiber's axial direction simulated for t=0.6 s and t=2.1 s, with Δx=500 μm (the label shows the position, in mm, and the temperature, in K, of the interception between plots), and (b) the variation on the interception point for different values of Δx (LPFG period). (P=6 W; t_{on}=0.6 s; Δt=1 s; F=0.461 N).

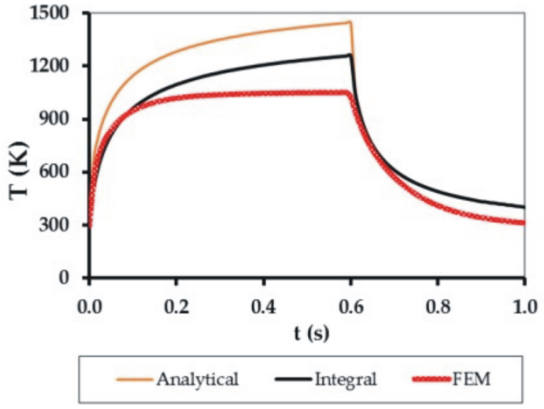

Figure 13. Plots of the temperature evolution during laser irradiation and cooling obtained using equations (11), analytical, and (8), integral, and the FEM model. (P=6 W; t_{on}=0.6 s; F=0.461 N).

http://dx.doi.org/10.5772/59153

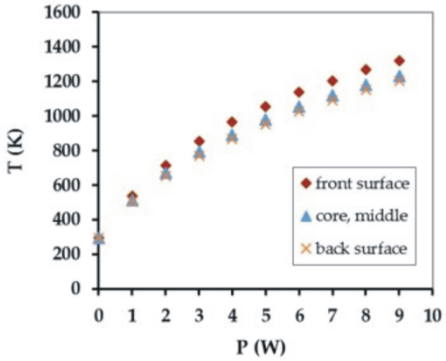

Figure 14. Maximum temperature calculated for different laser powers, at x=0 m. (P=6 W; t_{on}=0.6 s; F=0.461 N).

	a_3	a_2	a_1	a_0
Front surface	1.21	-26.64	256.4	295
Core, middle	1.06	-22.91	224.7	302
Back surface	0.97	-21.18	212.8	302

Table 2. Coefficients for equation (22), depending on the analysis point being considered (Figure 4).

Another parameter to take in consideration is the draw force due to the weight applied on the fiber. Figure 16 shows the behaviour of the refractive index change with the applied force (and corresponding weight), considering P=6 W and t_{on}=0.6 s. This parameter affects mainly the core and a linear relation (with F in N) can be obtained:

$$\Delta n_{\text{core}} = \left(-4.9388\,F + 0.0166\right) \times 10^{-4} \tag{23}$$

A microscope photograph of an example of an irradiated fiber under the experimental conditions considered in this work is shown in Figure 17. The imaged zone comprises one 500 μm period of a 25 mm grating irradiated with 6 W, for a duration of 0.6 s (each pulse) and subjected to a weight of 47 g. It is also visible a (small) micrometric deformation of the fiber in each irradiated region. Figure 18 shows the spectral transmission of the written LPFG, comparing the experimental data with the simulated spectrum, obtained using the refractive index changes calculated by the FEM model and using the simulation tool developed by Baptista [59].

In spite the relative spectral transmission data agreement, the experimental work demonstrated that different operational parameters can influence the resulting LPFG. In particular, the way the weight is positioned and laser power fluctuations can easily change the final result.

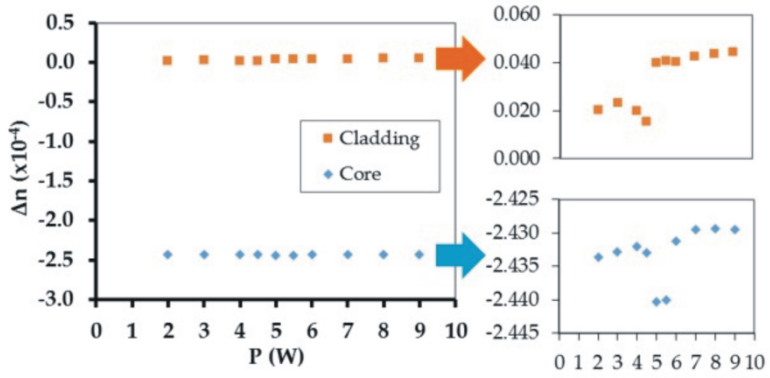

Figure 15. Calculated (maximum) refractive index change at the core and cladding for different applied laser powers. (t_{on}=0.6 s; F=0.461 N).

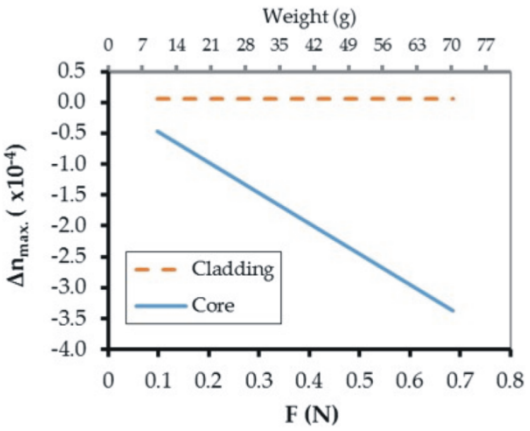

Figure 16. Calculated refractive index change (maximum change for core and cladding) for different applied draw tensions. (P=6 W; t_{on}=0.6 s; F=0.461 N).

In general, the process involves monitoring the transmission spectrum and iterative action on the length of the LPFG so a well-defined resonance is obtained. In our setup, the feedback on the emitted laser power reduces the problem, but not completely.

Although theoretically we could simulate considering different laser powers and weights, experimentally it was observed that using lower laser powers (<5 W) no LPFGs were obtained. Also, using higher laser powers (>8 W) or higher weights (typically >60 g, F > 0.6 N) tapering occurs, a phenomena not included in our model.

The values obtained by the model are in agreement with those estimated by other authors for the refractive index modulations necessary for achieving a fiber optic grating. Temperatures

http://dx.doi.org/10.5772/59153

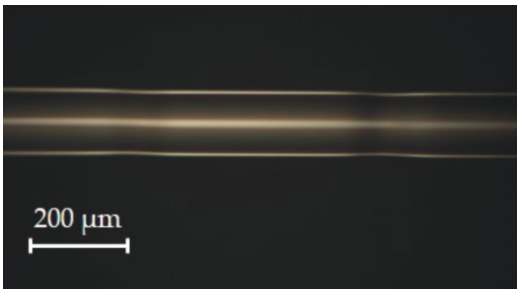

Figure 17. Picture showing two irradiated zones from a 25 mm LPFG with 500 μm period written on a SMF-28 optical fiber. ($P \approx 6$ W; t_{on}=0.6 s; Δt=1 s; $F \approx 0.5$ N)

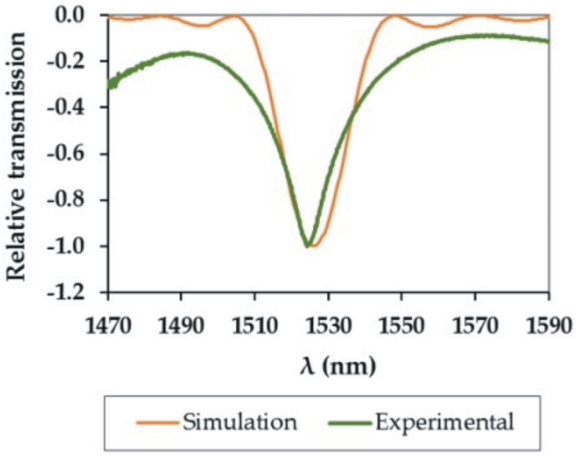

Figure 18. Experimentally obtained and simulated relative normalized spectral transmission under the same conditions considered in Figure 17.

calculated are similar to those obtained by other authors for arc-induced LPFG (e.g. in the range 1,100 K–1,400 K according to [56]) and the refractive index changes are within the overall range mentioned in other works [46,52,56]. Also, the behaviour of the refractive index change as the applied drawing force increases complies with recent experimental indications that the refractive index of the core decreases while the opposite occurs in the cladding, and that this change occurs primarily in the core [66,67].

Nevertheless, a complete model of the complex physical phenomena involved, in particular regarding the refractive index change dependence on stress, requires further research. It's expected that future work will focus on experimental measurements of temperature, stresses and refractive index changes induced by the MIR laser radiation. Also, although published works can contribute in assessing the validity of the results, the influence of specific charac-

teristics of the fibers is a well-recognized issue. In particular, the effect of pre-existing stresses (typically from the fiber manufacture or preparation), differences in the materials, or other unaccounted phenomena can influence the performance of the FEM model when compared with real data. Similarly, the impact of the several approximations considered (e.g., transverse stresses are neglected), unaccounted phenomena like eventual changes on the glass polarizability and using standard material data must be analysed in detail, as well as the influence of the experimental data uncertainties on the model.

5. Conclusions

In Summary, the CO_2 laser irradiation technique is a highly efficient, low cost and versatile technique to write high-quality LPFGs in different types of optical fibers, such as conventional single mode fibers, polarization-maintaining fibers, and photonic crystal fibers. This technique offers a number of advantages over other fabrication techniques. It eliminates the need of using a mask as well as the need for pre-hydrogenation of the fiber and consequent post-thermal annealing to stabilize the gratings. The LPFGs induced by CO_2 laser exhibits unique grating properties, such as high thermal stability.

Although simplifications can lead to analytical equations, FEM modelling allows more realistic simulations of the physical processes involved in the writing of LPFGs using MIR radiation. The 3D model presented simulates the writing of one period and allows the analysis of both thermal and stress data. All the main practical parameters are considered as inputs and thermal dependence of the material's data is included.

The model performance was evaluated by considering a practical example of writing LPFGs on a Ge-doped fiber. Different analysis were presented and it was demonstrated that refractive index changes predicted by the FEM model led to transmission spectra with resonance peaks similar to those obtained experimentally. So, although additional work should be performed to further validate the analysis done (mainly regarding the characterization of stresses acting in the optical fiber and experimentally measuring refractive index changes), the FEM results are in accordance with literature and experimental data.

Acknowledgements

This work was partially supported by FEDER funding through the Programa Operacional Factores de Competitividade – COMPETE and by national funding by the FCT – Portuguese Fundação para a Ciência e Tecnologia through the project PTDC/FIS/119027/2010. The authors gratefully acknowledge José Luis Santos, Orlando Frazão, Pedro Jorge and Paulo Caldas from INESC-Porto for their advices and crucial contributions. A special thanks to David Castro Alves, Fernando Monteiro and António Oliveira for their support to the experimental activities described in this chapter.

http://dx.doi.org/10.5772/59153

Author details

João M.P. Coelho[1,2], Catarina Silva[1], Marta Nespereira[1], Manuel Abreu[1] and José Rebordão[1]

1 Laboratório de Óptica, Lasers e Sistemas, Faculdade de Ciências, Universidade de Lisboa, Pólo do Lumiar, Estrada do Paço do Lumiar, Lisboa, Portugal

2 Instituto de Biofísica e Engenharia Biomédica, Faculdade de Ciências, Universidade de Lisboa, Campo Grande, Lisboa, Portugal

References

[1] Vengsarkar A, Lemaire P, Judkins J, Bhatia V, Sipe J. Long-Period Fiber-Grating-Based Gain Equalizers. Optics Letters 1996; 21(5):335-338.

[2] Das M, Thyagarajan K. Dispersion compensation in transmission using uniform long period fiber gratings. Optics Communications 2001; 190:159–163.

[3] Eggleton BJ, Slushe RE, Judkins JB, Stark JB, Vengsarkar AM. All-optical switching in long-period fiber gratings. Optical Letters 1997; 22(12): 883-885.

[4] Zhu C, Lu Y, Lacquet BM, Swart PL, Spammer SJ. Wavelength-tunable add/drop multiplexer for DWDM using long period gratings and fiber stretchers. Optics Communications 2002; 208(9): 337-344.

[5] Vengsarkar AM, Lemaire PJ, Judkins JB, Bhatia B, Erdogan T, Sipe JE. Long-period fiber gratings as band-rejection filters. In Optical Fiber Communication Conference, OFC95, San Diego, CA, Feb. 1995, PD4-2, 1995.

[6] Khaliq S, James S, Tatam R. Enhanced sensitivity fibre optic long period grating temperature sensor. Measurement Science and Technology 2002; 13(5):792–795.

[7] Patrick H, Chang C, Vohra S. Long Period Fiber Gratings for Structural Bend Sensing. Electronics Letters 1998;34(18):1773–1775.

[8] James S, Tatam R. Optical fibre long-period grating sensors: Characteristics and application. Measurement Science and Technology 2003;14:R49-R61.

[9] Bhatia V, Vengsarkar A. Optical fiber long-period grating sensors. Optics Letters 1996;21(9): 692-694.

[10] Patrick H, Kersey A, Bucholtz F. Analysis of the response of long-period fiber gratings to external index of refraction. Journal of Lightwave Technology 1998;16(9): 1606–1612.

[11] Silva C, Coelho J, Caldas P, Jorge P. Fibre Sensing System Based on Long-Period Gratings for Monitoring Aqueous Environments. In Yasin, M., Harun S, Arof H (Eds.) Fiber Optic Sensors. Ridjeka: InTech 2012. p317–342.

[12] Erdogan T. Fiber grating spectra. Journal of Lightwave Technology 1997;15(8): 1277-1294.

[13] Bhatia V. Applications of long-period gratings to single and multi-parameter sensing. Optics Express 1999;4(11): 457-466.

[14] Erdogan T. Cladding-mode Resonances in Short-and Long-period Fiber Grating Filters. Journal of the Optical Society of America A 1997;14(8): 1760-1773.

[15] Costa RZV, Kamikawachi RC, Muller M, Fabris JL. Thermal characteristics of long-period gratings 266 nm UV-point-by-point induced. Optics Communications 2009;282(5): 816-823.

[16] Zhang Y, Chen X, Wang Y, Cooper K, Wang A. Microgap Multicavity Fabry-Pérot Biosensor. Journal of Lightwave Technology 2007;25(7): 1797-1804.

[17] Lee CE, Gibler WN, Atkins RA, Taylor HF. In-Line Fiber Fabry-Pérot-Interferometer with High-Reflectance Internal Mirrors. Journal of Lightwave Technology 1992;10(10): 1376-1379.

[18] Nespereira M, Silva C, Coelho J, Rebordão J. Nanosecond Laser Micropatterning of Optical Fibers. In: Costa M. (ed.) International Conference on Applications of Optics and Photonics: proceedings of SPIE on CD-ROM: 8001, 3-7 May 2011, Braga, Portugal. Bellingham: SPIE 2011.

[19] Kawasaki BS, Hill KO, Johnson DC, Fujii Y. Narrow-band Bragg reflectors in optical fibers. Optical Letters 1978;3(2): 66–68.

[20] Douay M, Xie WX, Taunay T, Bernage P, Niay P, Cordier P, Poumellec B, Dong L, JF Bayron, Poignant H, Delevaque E. Densification involved in the UV-based photosensitivity of silica glasses and optical fibers. Journal of Lightwave Technology 1997;15(8):1329-1342.

[21] Fujimaki M, Nishihara Y, Ohki Y, Brebner JL, Roorda S. Ion-implantation-induced densification in silica-based glass for fabrication of optical fiber gratings. Journal of Applied Physics 2000;88(10): 5534-5537.

[22] Cardenas-Sevilla GA, Monzon-Hernandez D, Torres-Gomez I, Martinez-Rios A. Mechanically induced long-period fiber gratings on tapered fibers. Optics Communications 2009;282(14):2823-2826.

[23] Rego G, Okhotnikov O, Dianov E, Sulimov V. High-temperature stability of long period fiber gratings produced by using an electric-arc. Journal of Lightwave Technology 2001;19(10): 1574-1579.

[24] Humbert G, Malki A. High performance bandpass filters based on electric arc-induced π-shifted long-period fibre gratings. Electronics Letters 2003;39(21): 1506-1505.

[25] Nikogosyan D N. Long-period Gratings in a standard telecom fibre fabricated by high-intensity fentosecond UV and near-UV laser pulses. Measurement Science and Technology 2006;17(5): 960-967.

[26] Davis DD, Gaylord TK, Glytis EN, Kosinski SG, Mettler SC, Vengsarkar AM. Long Period Fibre Grating Fabrication with Focused CO_2 Laser Pulses. Electronics Letters 1998;34(3): 302-303.

[27] Kim BH, Ahn T, Kim DY, Lee BH,Chung Y, Un-Chul Paek, Won-Taek Han. Effect of CO_2 laser irradiation on the refractive-index change in optical fibers. Applied Optics 2002;41(19): 3809-3815.

[28] Akiyama M, Nishide K, Shima K, Wada A, Yamauchi R. A Novel Long-period Fiber Grating Using Periodically Releases Residual Stress of Pure-silica Core Fiber. In: Optical Fiber Communication Conference (OFC), San José, CA, pp. 276-277, Feb. 1998. [Techn. Dig. Conf. Opt. Fiber Commun., 276, 1998].

[29] Wang Y. Review of Long Period Fiber Gratings Written by CO_2 Laser. Journal of Applied Physics 2010;108(8): 081101.

[30] Rao YJ, Zhu T, Ran ZL, Wang YP, Jiang J, Hu AZ. Novel Long-period Fiber Gratings Written by High-frequency CO_2 Laser Pulses and Applications in Optical Fiber Communication. Optics Communications 2004;229(1-6): 209–221.

[31] Chan H, Perez E, Alhassen F, Tomov I, Lee H. Ultra-Compact Long-Period Fiber Grating and Grating Pair Fabrication using a Modulation-Scanned CO_2 Laser. In: Conference on Optical Fiber Communication and the National Fiber Optic Engineers Conference (OFC/NFOEC), Anaheim, CA, pp. 1-3, Mar. 2007. [Proc. of Nation Fiber Optic Engineers Conference, Optical Society of America, paper JWA5, 2007].

[32] Alves DC, Coelho J, Nespereira M, Monteiro F, Abreu M, Rebordão JM. Automation methodology for the development of LPFG using CO_2 laser radiation. In: Costa M. (ed.) 8th Iberoamerican Optics Meeting and 11th Latin American Meeting on Optics, Lasers, and Applications: proceedings of SPIE 8785, 18 November 2013: 6 pages.

[33] Ryu HS, Park YW, Oh ST, Chung YJ, Kim DY. Effect of asymmetric stress relaxation on the polarization-dependent transmission characteristics of a CO_2 laser-written long-period fiber grating. Optical Letters 2003;28(3): 155–157.

[34] Oh ST, Han WT, Paek UC, Chung Y. Azimuthally Symmetric Long-period Fiber Gratings Fabricated with CO_2 Laser. Microwave and Optical Technology Letters 2004;41(3): 188-190.

[35] Grubsky V, Feinberg J. Fabrication of axially symmetric long-period gratings with a carbon dioxide laser. IEEE Photonics Technology Letters 2006;18(21): 2296–2298.

[36] Zhu T, Chiang K, Rao Y, Shi C, Song Y, Liu M. Characterization of long period fiber gratings written by CO_2 laser in twisted single mode fibers. Journal of Lightwave Technology 2009. 27(21): 4863–4869.

[37] Shang RB. Fabrication of twisted long period fiber gratings with high frequency CO_2 laser pulses and its bend sensing. Journal of Optics 2013;15(7): 075402.

[38] Wang YP, Wang DN, W. jin, Rao YJ, Peng GD. Asymmetric long period fiber gratings fabricated by use of CO_2 laser to carve periodic grooves on the optical fiber. Applied Physics Letters 2006;89: 151105.

[39] Su L, KS Chiang, Lu C. CO_2-laser-induced long-period gratings in graded-index multimode fibers for sensor applications. *IEEE* Photonics Technology Letters 2006;18(1): 190–192.

[40] Kim CS, Han Y, Lee BH, Han WT, Paek UC, Chung Y. Induction of the refractive index changes in B-doped optical fibers through relaxation of the mechanical stress. Optics Communications 2000;185(4-6): 337-342.

[41] Kim BH, Park Y, Ahn TJ, Lee BH, Chung Y, Paek UC, Han WT. Residual stress relaxation in the core of optical fiber by CO_2 laser radiation. Optical Letters 2001;26(21): 1657-1659.

[42] Kakarantzas G, Birks TA, Russell PS. Structural long-period gratings in photonic crystal fibers. Optical Letters 2002;27(12): 1013–1015.

[43] Lee HW, Liu Y, ChiangKS. Writing of long-period gratings in conventional and photonic-crystal polarization-maintaining fibers by CO_2-laser pulses. IEEE Photonics Technology Letters 2008;20(2):132–134.

[44] Liu Y, Chiang KS. Recent development on CO_2-laser written long-period fiber gratings. In: V, Ming-Jun Li, Ping Shum, Ian H. White, Xingkun Wu, (eds.) Passive Components and Fiber-based Devices, proceedings of SPIE 7134: pp. 713-437,. Hangzhou, China October 26, 2008.

[45] Grellier AJC, Zayer NK, Pannell CN. Heat transfer modelling in CO_2 laser processing of optical fibers. Optics Communications 1998;152(4-6): 324-328.

[46] Yablon AD, Yan MF, Wisk P, DiMarcello FV, Fleming JW, Reed WA, Monberg EM, DiGiovanni DJ, Jasapara J. Refractive Index Perturbations in Optical Fibers Resulting from Frozen-in Viscoelasticity. Applied Physics Letters 2004;84(1):19-21.

[47] Coelho J, Nespereira M, Silva C, Rebordão J. Modeling refractive index change in writing long-period fiber gratings using mid-infrared laser radiation. Photonic Sensors 2013;3(1): 67-73, 2013.

[48] Coelho J, Nespereira M, Silva C, Rebordão J. 3D Finite Element Model for Writing Long-Period Fiber Gratings by CO_2 Laser Radiation. Sensors 2013;13(8): 10333-10347.

[49] Coelho J, Nespereira M, Silva C, Pereira D, Rebordão J, Advances in optical fiber laser micromachining for sensors development, In: Sulaiman Wadi Harun and Ham-

zah Arof (Eds.) Current Developments in Optical Fiber Technology. Ridjeka: Intech; 2013. p375-401.

[50] Coelho J, Abreu MA, Carvalho-Rodrigues F. Modelling the spot shape influence on high-speed transmission lap welding of thermoplastics films. Journal of Optics and Lasers in Engineering 2008;46(1): 55-61.

[51] Yang S, Matthews M, Elhadj S, Draggoo, V, Bisson S. Thermal transport in CO_2 laser irradiated fused silica: in situ measurements and analysis. Journal of Applied Physics 2009;106: 103-106.

[52] Yablon AD. Optical and Mechanical Effects of Frozen-in Stresses and Strains in Optical Fibers. IEEE Journal of Selected Topics in Quantum Electronics 2004;10(2): 2004.

[53] Timoshenko SP, Goodier JN. Theory of elasticity, 2nd Ed.; New York: McGraw-Hill; 1970. p409-410.

[54] Hibino Y, Hanawa F., Abe T, Shibata S. Residual stress effects of refractive indices in undoped silica-core single-mode fibers. Applied Physics Letters 1987;50(22): p1565-1566.

[55] Hibino Y, Edahiro T, Horiguchi T, Azuma Y, Shibata N. Evaluation of residual stress and viscosity in SiO_2-core/F-SiO_2 clad single mode fibers from Briouin gain spectra. Journal of Applied Physics 1989;66(9): 4049-4052.

[56] Rego, GM. Arc-induced long-period fibre gratings. Fabrication and their application in communications and sensing. Ph.D. dissertation, Dept. Elect. Comp. Eng., Univ. of Porto, Porto, Portugal, 2006.

[57] Lancry, M, Réginier, E, Poumellec, B. Fictive temperature in silica-based glasses and its application to optical fiber manufacturing. Progress in Material Sciences 2012;57: 63-94.

[58] Corning® SMF-28 optical fiber product information. New York: Corning Inc.: 2002.

[59] Baptista, FDV Simulação do Comportamento Espectral de Redes de Período Longo em Fibra Óptica. Ms. dissertation, Centro de Ciências Exactas e da Engenharia, Univ. of Madeira, Funchal, Portugal, 2009.

[60] Erdogan, T. Cladding-mode resonances in short-and long-period fiber grating filters: errata. Journal of the Optical Society of America A 2000;17: p2113.

[61] McLachlan A, Meyer F. Temperature dependence of the extinction coefficient of fused silica for CO_2 laser wavelengths. Applied Optics 1987;26(9):p1728–1731.

[62] André P, Rocha A, Domingues F, Facão M. Thermal effects in optical fibers. In Marco Aurélio dos Santos Bernardes (Ed.) Developments in Heat Transfer; Ridjeka: Intech; 2011. p1–20.

[63] Clowes J, Syngellakis S, Zervas M. Pressure sensitivity of side-hole optical fiber sensors. IEEE Photonics Technology Letters 2009;10(6): 857–859.

[64] Siegman AE, Sasnett MW, Johnston TF. Choice of clip level for beam width measurements using knife-edge techniques. IEEE Journal of Quantum Electronics 1991;27(4): 1098–1104.

[65] Nespereira M, Alves, DC, Monteiro, F, Abreu, M, Coelho J, Rebordão JM. Repeatability analysis on LPFGs written by a CO_2 laser. In: Costa M. (ed.) II International Conference on Applications of Optics and Photonics: proceedings of SPIE 9286, 26-30 May 2014, Aveiro, Portugal. Bellingham: SPIE 2014.

[66] Li Y, Wei T, Montoya JA, Saini SV, Lan X, Tang X, Dong J, Xiao H. Measurement of CO_2-laser-irradiation-induced refractive index modulation in single-mode fiber toward long-period fiber grating design and fabrication. Applied Optics 2008;47(29): 5296-5304.

[67] Hutsel MR, Gaylord TK. Residual-stress relaxation and densification in CO_2-laser-induced long-period fiber gratings. Applied Optics 2012;51(25): 6179-6187.